4th MASHCON, Hamburg - Uliczka et al. (eds) - © 2016 Bundesanstalt für Wasserbau ISBN 978-3-939230-38-0 (Online)
DOI: 10.18451/978-3-939230-38-0_9

NUMERICAL SIMULATION OF THE SHIP BOTTOM INTERACTION OF DTC CONTAINER CARRIER FOR DIFFERENT KEEL CLEARANCE IN PURE SWAY MOTION

R He, **Z Z Zhang, X Z Wang** and **D K Feng,** School of Naval Architecture and Ocean Engineering, Huazhong University of Science and Technology, P. R. of China

SUMMARY

In this paper, numerical simulations were performed to study the hydrodynamic behavior of DTC container carrier under the same conditions with the experimental set up and operation conditions. In order to predict ship motion with larger amplitude, overset grid generation technology was used during the simulation. For ship-bottom interaction, the mean running sinkage and trim are major concerns during the Planar Motion Mechanism (PMM) test as well as forces and moment measurement. Therefore, the 3DOF module is applied in the numerical simulation. The heave and pitch motions are predicted by solving the equations of motions on each time step based on the hydrodynamic forces obtained from the solver. A good correspondence between the measured and simulated result is noted, indicating that forces and moments on the ship are well predicted. In the second stage, a set of systematic computations is carried out to study the ship-bottom interaction with different depth. The forces and moments on the hull with varying water depth are predicted and explained.

NOMENCLATURE

B	Beam (m)
Cfx	Coefficient of non-dimensional surge force
Cfy	Coefficient of non-dimensional sway force
Cmz	Coefficient of non-dimensional yaw moment
D	Depth (m)
Fr	Froude number based on L_{pp} (-)
Fr_{crit}	Critical value of Froude number (based on water depth) accounting for blockage(-)
h	Water Depth (m)
L_{pp}	Length between perpendiculars (m)
L_m	Length of the ship model (m)
$O_0x_0y_0z_0$	Earth-bound reference system
$Oxyz$	Ship-bound reference system
$O'x'y'z'$	Horizontal bound towing carriage System
p	Roll velocity (rad/s)
q	Pitch velocity (rad/s)
r	Yaw velocity (rad/s)
t	Time (s)
T	Time period (s)
Tm	Mean draft (T)
u	Longitudinal velocity component (m/s)
v	Lateral velocity component (m/s)
v_{max}	Maximum lateral velocity component(m/s)
w	Vertical velocity component (m/s)
y_{max}	Maximum lateral position (m/s)
β	Drift angle (deg)
φ	Roll angle (deg)
θ	Pitch angle (deg)
ψ	Course angle (deg)
AP	Aft Perpendicular
CG	Centre of Gravity
DTC	Duisburg Test Case
FP	Fore Perpendicular
UKC	Under Keel Clearance
▽	Displacement (m^3)

1 INTRODUCTION

Nowadays, Computational Fluid Dynamics (CFD) is being used as an efficient design tool to predict the maneuvering characters of a ship. Increasing ship sizes in all dimensions and optimizations in the design and maintenance of waterways, request clearer understanding of the interaction between a ship hull and the bottom of the waterways helps to improve the maneuvering performance and increase the security of operation. Therefore, ship-bottom interaction is significantly important for the navigation. Particularly in restricted water the interaction can be stronger, and the problem may also be crucial for the waterways and harbor design. Due to these facts, ship-bottom interaction has been the focus in many ways for a long time. In general, most of the investigations still rely on empirical formula, experimental tools as well as numerical simulations, among which the first two types are more widely used. In this article, the planar motion mechanism (PMM) simulation is employed using an in-house RANS solver.

Table 1. Effect of depth restrictions[1]

Definitions	Ratio	Depth restrictions
Deep water	$h/T_m>3.0$	No effect
Medium deep water	$1.5<h/T_m<3.0$	Noticeable
Shallow water	$1.2<h/T_m<1.5$	Very significant
Very shallow water	$h/T_m<1.2$	Dominates the behavior

In shallow water, the clearance under the vessel becomes smaller, resulting in an increase of the current loads due to the blockage effect. The ratio of water depth to draft is used to evaluate the depth restrictions. Table 1 shows the details of effect of depth restrictions.

Among several methods for maneuvering characters prediction, PMM tests are the most commonly accepted approaches.
However, the tests contain several disadvantages; (1) the expensive test facilities and sophisticated experimental settings; (2) considerable scale effect resulting from the impossibility in practice to achieve Froude number and Reynolds number similarities simultaneously; (3) limitations in obtaining details of flow fields around the ship. CFD based maneuvering prediction methods significantly manage to resolve these problems as the viscous effects
are very important for accurate maneuvering prediction.
SIMMAN2008 [2] and SIMMAN2014 maneuvering workshop benchmarks the prediction characters of ship maneuvering using both system-based and CFD-based methods. Broglia [3] demonstrated the capability of CFD prediction for dynamic PMM simulations of KVLCC1/KVLCC2 with appendage. KumarPatel [4] investigated the shallow water effect on the wave pattern using a commercial Rans solver starccm+. Liu [5] extends a new 6DOF module and simulate the oblique towing tests, while the shallow water effect is also taken into account. These studies showed that CFD can improve the modeling of ship hydrodynamics. Sakamoto [6] and Yoon [7] present the benchmark CFD validation measurements for surface combatant 5415, both experiment and simulation results are mathematically formulated by Fourier series method to obtain expressions of the hydrodynamic derivatives.
In this paper computations are presented for the ship-bottom interaction in a small UKC. The CFD results are shown to accurately match the experimental results. Blockage effects and scale effects are known issues when carrying out model tests for shallow water but these effects can be efficiently quantified with CFD.
Furthermore, a series of systematic computations with a wide range of UKC are presented to provide more extensive knowledge about the ship-bottom interaction.

2 BENCHMARK DESCRIPTION

The model ship used for this research is the Duisburg Test Case (DTC) [8][9] container ship, which is a 14,000 TEU capacity container ship developed by Institute of Ship Technology, Ocean Engineering and Transport Systems for research purpose, including the benchmarking and validation of numerical method. The Planar Motion Mechanism tests include both static test and dynamic tests that have been executed with a scale model of DTC container ship in the Towing Tank for Maneuvering in Shallow Water at Flanders Hydraulics Research, Antwerp Belgium.
The geometric characteristics of the DTC model are presented in [9] The length between perpendiculars is 3.984m with a scale factor 1/89.11. The DTC container ship was equipped with a twisted rudder with a costa bulb, and with a pitch-fixed five-bladed propeller. The geometries of both hull and appendage are illustrated in Figure 1. For the dynamic PMM simulations, the ship has prescribed lateral velocity in pure sway motion and rotation velocity around Z axis as well as lateral velocity in pure yaw motion. Table 2 lists the principal dimensions of the vessel for the model used in the PMM tests. In the benchmark test, static draft and dynamic PMM tests have been performed, for both test two model speed are tested. It should be noted that only detailed test data of pure sway and pure yaw are given by the experiments.

Table 2. Principal Dimensions of vessel

Ship parameter		Full Scale	Model Scale
Scale	λ	1	89.11
Lpp	m	355	3.984
B	m	51	0.572
d	m	14.5	0.163
∇	m^3	173.925	0.2458

Figure 1. DTC Hull Form

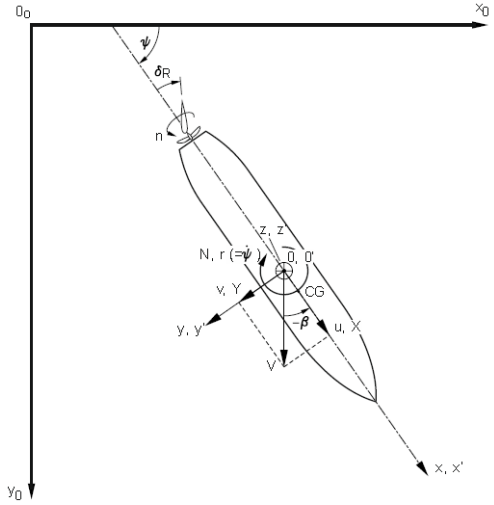

Figure 2. PMM test coordinate system

The coordinate system utilized for PMM test is given by Figure 2 [9] Two coordinate system are used in the experimental test, $O_0x_0y_0z_0$ represents the earth-fixed coordinate system and be used for towing carriage, Oxyz is the ship-fixed coordinate system, and center is at mid-point of the ship (0.5Lpp from AP to FP). O'x'y'z' is used during experimental test and thus also during ship hydrodynamics simulation based upon model test. In the ship-fixed coordinate system, x axis follows from stern towards bow direction, y axis follows from middle towards starboard, z axis follows from the waterline towards the keel.
During the pure sway test, the ship axis is always parallel along with the velocity direction of the free-steam, the longitudinal speed u takes a constant value, while the sway position y, sway velocity v and sway acceleration $\dot{v}$ as a function of time.

$$\begin{cases} y = y_{max}cos(\omega t) \\ v = -v_{max}sin(\omega t) \\ \dot{v} = -\dot{v}_{max}cos(\omega t) \end{cases} \quad (1)$$

where $\omega_{sway} = 2\pi/T$ is the angular frequency of sway motion, v_{max} is the maximum sway velocity, and $\dot{v}_{max}$ is the maximum sway acceleration.

3 RANS SOLVER

3.1 DYNAMIC OVERSET

The overset grid technique is adopted to simulate dynamic ship motion and grid refinement, the overset grid technique provides the ability of separate grids independently moving without restrictions. The in-house overset software os-grid written by Fortran is used to obtain the grid connectivity information. For the dynamic PMM simulation in this paper, the relative position between overset grids change very time step, requiring regeneration of the grid connectivity information in every step time. While simulation starts, flow variables (velocity, force, pressure, density function) exchange information between the RANS solver and the overset solver at every time step. Firstly, the RANS solver computers the basic flow parameter, and then os-grid searches for the point located in the overlapping domain. Secondly, the forces and moments will transmit to the inner grid, as well as the motions predicted by the first step. Flow parameter in the inner grid finishes its iteration and send the flow information back to the outer grid by os-grid. By repeating the process every time step, the RANS solver can finish the PMM test trim and sinkage prediction.

Unlike the general overset grid assembly software SUGGAR [10], os-grid can only handle with structured grids and lacks the capability for generating the grid connectivity information in parallel computers. Since the generation of the grid connectivity information on structured grid is much more fast than on an unstructured grid, the time spent on the exchange of information is acceptable. But the promotion of the efficiency will be an important part of the future work. Serial and parallel performance of the code is still being investigated and improved and will not be discussed in this paper.

3.2 GOVERNING EQUATIONS

The viscous flow is represented by the non-dimensional incompressible unsteady Reynolds-Averaged Navier-Stokes (URANS) equations coupled with the time-averaged continuity equation:

$$\begin{cases} \frac{\partial \bar{u}_i}{\partial t} + \bar{u}_j \frac{\partial \bar{u}_i}{\partial x_j} + \frac{\partial \bar{p}}{\partial x_i} - \frac{1}{Re}\frac{\partial^2 u_i}{\partial x_j \partial x_j} - \frac{\partial}{\partial x_j}\left(-\rho \overline{u_i' u_j'}\right) = 0 \\ \frac{\partial \bar{u}_i}{\partial x_i} = 0 \end{cases} \quad (2)$$

Where $\bar{u}_i$, $\bar{u}_j$, $\bar{p}$ denote the average velocity, pressure, respectively. $-\rho\overline{u_i' u_j'}$ denotes the Reynolds stresses, u_i' represents the fluctuating velocity in time.

In addition, the two-equation shear stress transport (SST) model is employed to close the RANS equations:

$$\begin{cases} v_t = \frac{k}{\omega} \\ \frac{\partial k}{\partial t} + \left(U_j - \sigma_k \frac{\partial v_t}{\partial x_j}\right)\frac{\partial k}{\partial x_j} - \frac{1}{R_k}\nabla^2 k + s_k = 0 \\ \frac{\partial \omega}{\partial t} + \left(U_j - \sigma_\omega \frac{\partial v_t}{\partial x_j}\right)\frac{\partial k}{\partial x_j} - \frac{1}{R_\omega}\nabla^2 \omega + s_\omega = 0 \end{cases} \quad (3)$$

The control equations adopted cell-centered finite differential. The discretization of time terms in implemented by 2nd Euler backward difference scheme. In eq.3, the discretization of convective terms is implemented by 2nd upwind differences scheme and for the diffusive fluxes central differences are applied.

3.3 MANEUVERING SIMULATION

A motion of five degrees of freedom (5 DOF) was adopted in the simulation. The rigid-body equations described in eq.4 written in a hybrid coordinate system have determined the motions excepting roll.

$$\begin{cases} X = m[\dot{u} - rv + wq - x_G(q^2 + r^2) + z_G\dot{q}] \\ Y = m(\dot{v} + ru + z_G qr + x_G\dot{r}) \\ N = I_z\dot{r} + mx_G(\dot{v} + ur) \end{cases} \quad (4)$$

Where u, v and w are the surge, sway and heave velocity in the longitudinal, lateral and vertical directions of the earth-fixed coordinate system, respectively. $\dot{u}$, $\dot{v}$ are accelerations. q and r are the angular velocity rotations around the axes x and axes z, respectively. $\dot{q}$ and $\dot{r}$ are the pitch and yaw accelerations, respectively. x_G, z_G are the location of the center of gravity of the vessel. I_z are the mass and moment of inertia of the model.

3.4 COMPUTATIONAL DOMAIN AND GRIDS

The computational domain for benchmark test study is made up by various boundaries as follows: inlet plane in front of the bow, outlet plane behind the tail, no-slip conditions are applied on the hull, relative-frame no-slip conditions are applied for both the bottom and side. The domain extend from xmin = -Lpp to xmax = 3Lpp on axis x, from ymin = -3.5m to ymax = 3.5m on axis y and from zmin = -0.196 to zmax = 0.2Lpp on axis z, respectively.

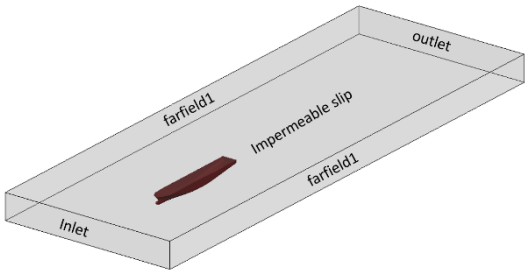

Figure 3. Solution domain and boundary conditions

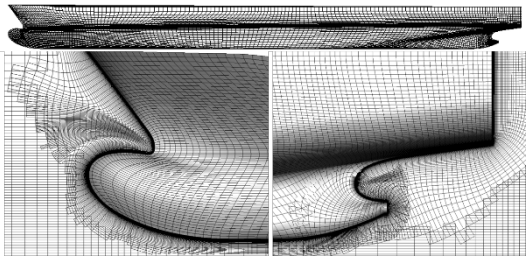

Figure 4. Overset grid near the bulb, stern and in gap between ship and bottom

The grids were generated by Pointwise for different UKC, with h/T = 1.2 representing very shallow water, h/T = 1.5 representing shallow water, h/T = 3 representing middle deep water and h/T = 10 representing deep water. There are two different grid blocks for each set: inner grid for hull, outer grid for background. With the dynamic overset technology, the inner grid topology around the hull for the four water depths was the same, the outer grid topology are similar except for the water depth between the keel and bottom. The inner grid is generated with a hyperbolic grid generator using C-type topology. In this study, no wall function is used, the minimum size of the grid cell for boundary layer should be refined to 10e-6 as the SST $k-\omega$ turbulence model was adopted and maximum y+ value around the hull is less than 1. The outer grid is generated using H-type grid topology. The total number of grid points is 4.1M.

3.5 GRID SENSITIVITY INVESTIGATION

To investigate the sensitivity of the results to the grid resolution, three sets of grids with 2.3M, 4.1M and 9.7M are used in the preliminary study. The grid densities are systematically vary as a refinement ratio 1.4 at each directions. A comparison of resistance coefficient is shown in Table 3, the inlet velocities of various are at 0.599m/s and 0.872m/s respectively. As can be seen, there is lightly difference between the medium and fine meshed and the computation values of resistance are in good agreement with the experimental values. Thus, the medium mesh with about 4.1M is selected as the final grid in the PMM simulation.

Table 3. A comparison of coefficient of resistance of the DTC at different Fr values

V (m/s)	Coefficient of total resistance at different Fr values (10e-3)		
	Coarse mesh(2.3 M)	Medium mesh (4.1 M)	Fine mesh (9.7M)
5.99	6.82	6.79	6.78
8.72	7.30	7.28	7.28

4 RESULTS AND ANALYSIS OF HYDRODYNAMIC DERIVATIVES

4.1 NON-DIMENSIONALISED OF PARAMETERS

All the fluid variables are transmitted to a non-dimensional form with respect to the advancing velocity of ship u, the ship length *Lpp* and the fluid density ρ. The relations between non-dimensional parameters and dimensional ones can be seen in the following equations.

$$time, t^* = t\left(\frac{u}{Lpp}\right)$$

$$position,\ x^* = \frac{x}{Lpp}$$

$$velocity, v^* = \frac{v}{u}$$

$$acceleration, \dot{v}^* = \frac{v}{u^2}$$

$$force, F^* = \frac{F}{0.5\rho u^2 Lpp^2}$$

$$Moment, M^* = \frac{M}{0.5\rho u^2 Lpp^3}$$

$$Pressure, p^* = \frac{pLpp}{\rho u}$$

4.2 PURE SWAY MOTION

Comparisons between numerical simulation results and experimental results will be presented for the resistance coefficient Cfx, sway resistance coefficient Cfy, yaw moment coefficient Cmz, as well as the sinkage and trim. Test 2016_C and Test 2016_D have the same under-keel-clearance (UKC) and motion frequency, but the inlet velocity u is different. The pure sway test can be used to determine derivatives of $Y_{\dot{v}}$ and $N_{\dot{v}}$, as well as the Y_v and N_v. However, Y_v and N_v can also be determined from the static PMM test, and results through static test are more accurate and convenient to obtain in general.

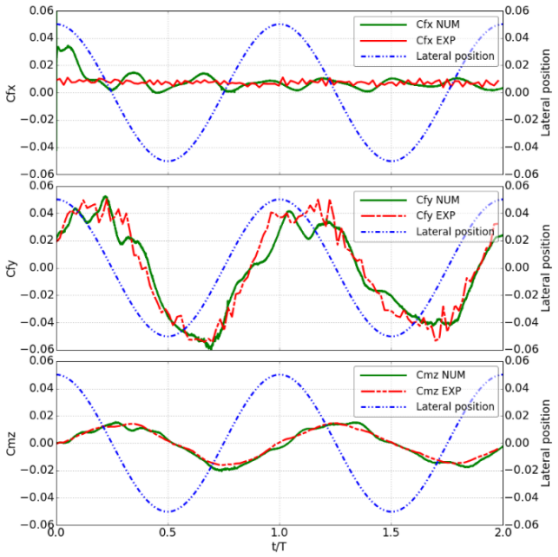

Figure 5. Time-history of coefficient of force and moment over 2 periods for DTC in pure sway motion, free to heave and pitch (u=0.599m/s)

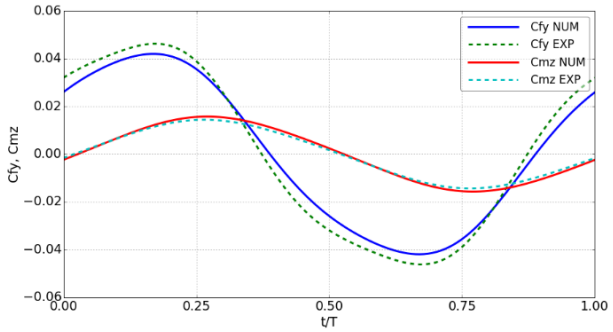

Figure 6. Time-history of coefficient of force and moment over 1 period for DTC in pure sway motion, free to heave and pitch (u=0.599m/s)

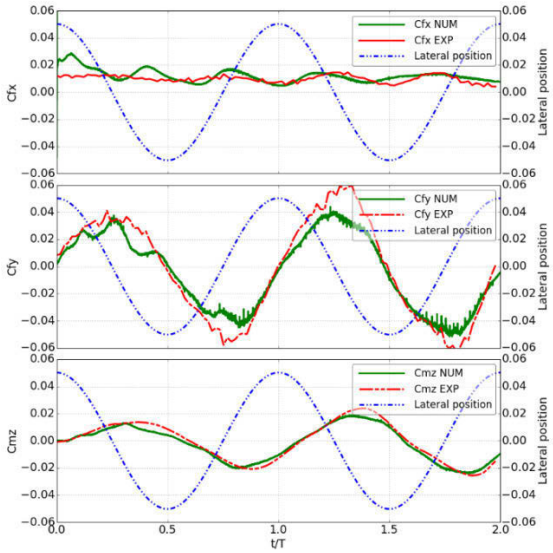

Figure 7. Time-history of coefficient of force and moment over 2 periods for DTC in pure sway motion, free to heave and pitch (u=0.872m/s)

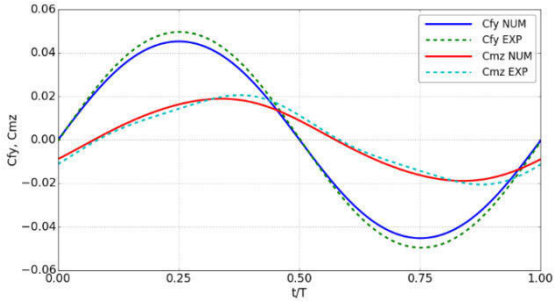

Figure 8. Time-history of coefficient of force and moment over 1 period for DTC in pure sway motion, free to heave and pitch (u=0.872m/s)

For each force and moment, the results are presented as non-dimensional time history type. Figure 5 and Figure 7 show the CFD pure sway test compared with the experimental test of resistance coefficient Cfx, total lateral force coefficient Cfy and yaw moment coefficient Cmz for Test 2016_C and Test 2016_D, respectively. In these figures, the raw curve from the simulation in two motion cycles has been used for analysis. Figure 6 and Figure 8 are also the Cfy and Cmz comparisons, only for the curves have been fitted using Fourier series, for both the simulation and experimental results.

Table 4. Hydrodynamic derivatives value for the pure sway motion

	u=0.599m/s			u=0.872m/s		
	EFD	CFD	E%	EFD	CFD	E%
Y_v	-0.2186	-0.2585	18.2	-0.7154	-0.6555	8.3
N_v	-0.1214	-0.1329	9.4	-0.2975	-0.2487	16.4
$Y_{\dot{v}}$	-0.1461	-0.1186	18.8	0.0066	0.0016	75.3
$N_{\dot{v}}$	0.0075	0.0110	46.7	0.1092	0.0864	20.9

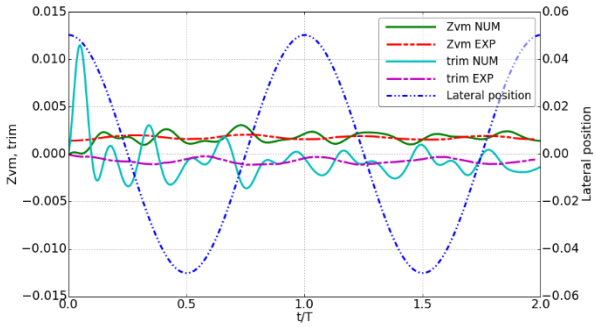

Figure 9. Time-history of mean sinkage and trim over 2 periods for DTC in pure sway motion (u=0.599m/s)

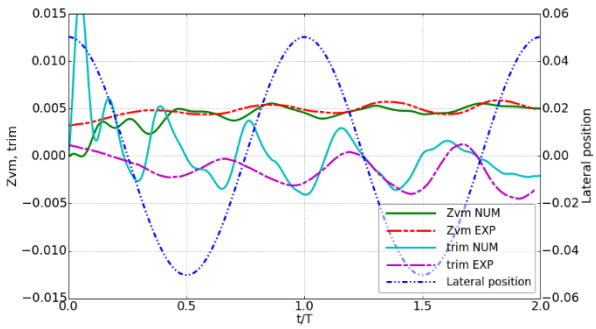

Figure 10. Time-history of mean sinkage and trim over 2 periods for DTC in pure sway motion (u=0.872m/s)

Figure 9 shows the comparison of the motion tendency of sinkage and trim with respect to non-dimensional time. Results for both sinkage and trim are almost the same after the simulation get stable. In common with comparison in Figure 5 - Figure 10, using simulation for pure sway shows high feasibility, accuracy and acceptable time consumption. The overall trend shows that the computational results agree well with the experimental data. It implies that the numerical simulation of pure sway test can be an alternative option to the experiment. Normally, $Y_{\dot{v}}$ is negative, but it increases to a positive value when the velocity gets close to the critical velocity, and the value is very close to zero, thus E% errors of the derivative $Y_{\dot{v}}$ get larger.

4.3 SYSTEMATIC COMPUTATIONS

In the previous sections, the ship-bottom interaction in very shallow water has been studied for four benchmark test cases. The comparison included resistance, lateral forces and yaw moment, and provided sinkage and trim. However, the trend with respect to various UKC is not clear. More over in the real situation, specifically during the motion in the harbor, the ship-bottom interaction often takes place in a complex situation with different UKC. Therefore, it would be worthwhile to study the ship-bottom interaction from a more general perspective.
The systematic computations were performed applying the same motion as in the preliminary benchmark case study, and the results will be reported as follows.
By using overset method, the grid topology around the hull for the four water depths was the same. The difference is the overset region between the bottom and the hull, as shown in Figure 11.

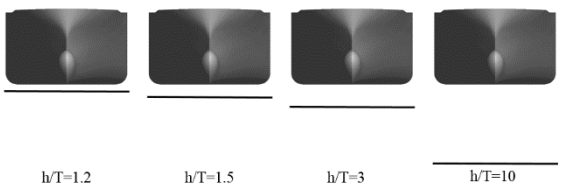

Figure 11. Different water depth considered in the systematic computations

Table 5. Matrix of simulation conditions for systematic computations

Conditions	Pure Sway				
Test no.	C	D	E	F	G
h/T_m	1.2	1.2	1.5	3.0	10
Speed(m/s)	0.599	0.872	0.872	0.872	0.872
Fr	0.096	0.139	0.139	0.139	0.139
Re (10e-6)	2.381	3.463	3.463	3.463	3.463
ymax(m)	0.2	0.2	0.2	0.2	0.2
Drift Angle(deg)	6.004	4.132	4.132	4.132	4.132
T(s)	20	20	20	20	20

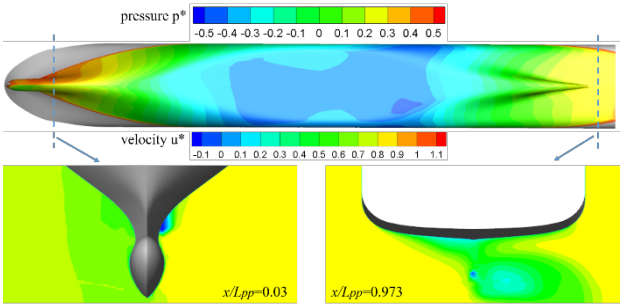

Figure 12. Pressure distributions on the bottom of DTC and velocity distributions on two slices in simulation case D (h/T = 1.2)

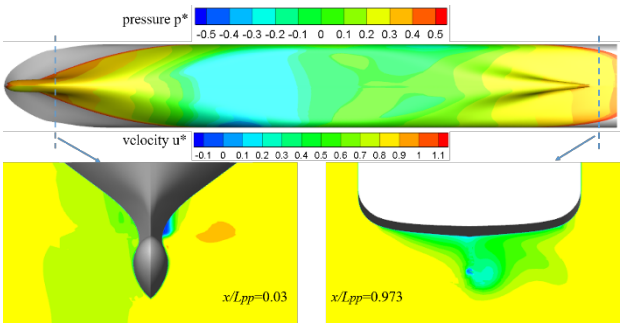

Figure 13. Pressure distributions on the bottom of DTC and velocity distributions on two slices in simulation case E(h/T = 1.5)

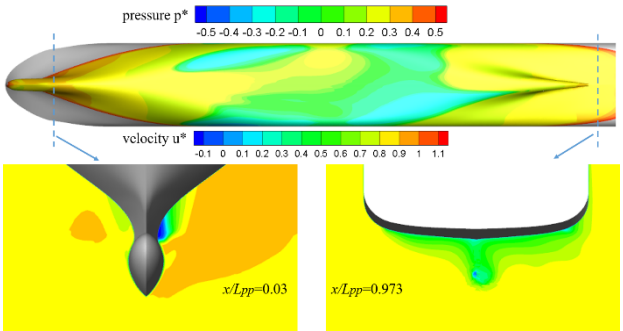

Figure 14. Pressure distributions on the bottom of DTC and velocity distributions on two slices in simulation case F (h/T = 3.0)

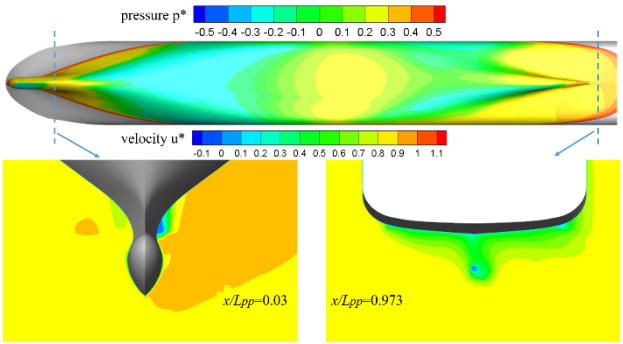

Figure 15. Pressure distributions on the bottom of DTC and velocity distributions on two slices in simulation case G (h/T = 10)

Figure 12, Figure 13, Figure 14 and Figure 15 show the pressure distributions on the keel and the averaged axial velocity at two slices along the longitudinal direction.
In case D (Figure 12), the suction peak (i.e. negative pressure region) is located at the middle of the bottom. Therefore there is an additional resistance, tending to increase the lateral force and the sinkage. For the velocity distributions on the slice at x/lpp = 0.973, there is a clear hook-shape pattern.
In contrast with case D, in case E (Figure 13) the negative pressure region on the middle-body is moving to the fore-body and the value of the pressure is increased over the entire bottom. Furthermore, the pressure difference is reduced at the bow.
As in case F (Figure 14) and case G (Figure 15), there is a positive pressure region located at the middle of the

ship. The velocity distributions on the slice located at the bulb and stern show the same characteristics.
The tendency of Cfy and Cmz for ratio h/Tm is shown in Figure 16, and the tendency of the non-dimensional sinkage and trim for ratio h/Tm is shown in Table 6.

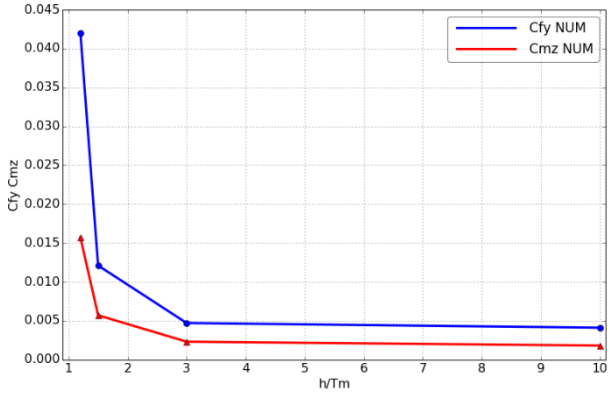

Figure 16. Tendency of Cfy and Cmz for ratio h/Tm

Table 6. Matrix of simulation results for systematic computations vs. expriments

Test no.	D exp	D	E	F	G
Zvm*(10e-3)	-4.833	-4.855	-3.012	-1.139	-0.489
Trim*(10e-3)	-1.464	-1.039	-1.424	-0.900	-0.786

5 CONCLUSIONS

The paper includes Planar Motion Mechanism (PMM) test results produced using CFD and compares with experimental data. It also discusses the hydrodynamic derivation from the simulated PMM results and compares them with the values from the test. These results show good agreement in pure sway cases, some discrepancy is observed, which may be attributed to the complex motion. The predicted pressure distribution on the hull and on the surface in one motion period was used to explain the lateral force and yaw moment acting on the hull. There was also a good correspondence between the two sets of PMM simulations both for trim and sinkage, despite for the difference in Cfy as mentioned above. However, the difference of lateral force Cfy between the simulation results and experimental results with the smallest UKC was relatively large and needs further studying. A detailed error analysis in both computations and measurements should be of great value.
Based on the benchmark validation study, an investigation about PMM simulations with different UKC was made. In the investigation, the forces and moments in the variation were predicted. Furthermore, the axial wake fields and the axial velocity contours on the slices along the longitudinal direction illustrated the ship-bottom interaction with varying UKC. In this way, resulting trends of the systematic computations could be explained. The forces and moments all decreased as the UKC was increased, and the changes on the forces were most significant. The sinkage and trim also decreased as the UKC was increased, while for the change was relatively small.

6 ACKNOWLEDGEMENTS

The authors thank Flanders Hydraulics Research and the Maritime Technology Division, Ghent University, Belgium, for providing the ship-bottom interaction benchmark test data.

7 REFERENCES

1. PIANC (1992). Capability of Ship Manoeuvring Simulation Models for Approach Channels and Fairways in *Harbours: Report of Working Group No. 20 of Permanent Technical Committee II*.

2. Stern, F.; Agdrup , K. (2008). SIMMAN 2008 workshop on verification and validation of ship maneuvering simulation method. *Proceedings of SIMMAN 2008 workshop on verification and validation of ship maneuvering simulation methods*, Lyngby, Denmark.

3. Broglia, R.; Muscari, R.; Di Mascio, A. (2008). Numerical simulations of the pure sway and pure yaw motion of the KVLCC1 and 2 tanker. *Proceedings of SIMMAN 2008 workshop on verification and validation of ship maneuvering simulation methods*, Lyngby, Denmark.

4. Patel, P..K.; Premchand, M. (2015). Numerical Investigation of the Influence of Water Depth on Ship Resistance. *International Journal of Computer Applications* 116: pp. 10-17

5. Liu, X.; Wan, D. (2015). Numerical Simulation of Ship Yaw Maneuvering in Deep and Shallow Water. *The Twenty-fifth International Offshore and Polar Engineering Conference*, Hawaii, USA.International Society of Offshore and Polar Engineers: pp. 21-26

6. Sakamoto, N.; Carrica, P. ; Stern, F. (2012). URANS simulations of static and dynamic maneuvering for surface combatant: part 1. Verification and validation for forces, moment, and hydrodynamic derivatives. *Journal of Marine Science and Technology* 17: pp. 422-445. doi:10.1007/s00773-012-0178-x

7. Yoon, H.; Simonsen, C.; Benedetti , L.; Lon-go, J. ; Toda, Y. ; Stern, F. (2015). Benchmark CFD validation data for surface combatant 5415 in PMM maneuvers–Part I: Force/moment/motion measurements. *Ocean Engineering* 109: pp. 705–734. doi:10.1016/j.oceaneng.2015.04.087

8. el Moctar, O.; Shigunov, V.; Zorn, T. (2012). Duisburg Test Case: Post-panamax container ship for benchmarking. *Ship Technology Research* 59: pp. 50-64.

9. Eloot, K.; Vantorre, M.; Delefortrie, G.; Lataire, E. (2016). Running Sinkage and Trim of the DTC Container Carrier in Harmonic Sway and Yaw Motion: Open

Model Test Data for Validation Purposes. *Fourth International Conference on Ship Manoeuvring in Shallow and Confined Water (MASHCON): Ship - Bottom Interaction*, 23-25 May 2016, Hamburg, Germany.

10. Noack, R. (2005). SUGGAR: a general capability for moving body overset grid assembly. *17th AIAA Computational Fluid Dynamics Conference*, Toronto, Ontario, Canada.

8 AUTHORS BIOGRAPHIES

Ran He is a research student, pursuing Ph.D., in School of Ocean Engineering, Huazhong University of science and technology. His area of research is Numerical study of surface ship maneuvering.

Zhiguo Zhang holds the position of Professor School of Ocean Engineering, Huazhong University of science and technology. He has more than 20 years' experience in teaching and research related to Naval Architecture and Ocean Engineering. His major fields of interest are ship maneuvering and motions, propeller performance and ocean wave-structure interaction.

Xianzhou Wang is a lecturer and research fellow in School of Ocean Engineering, Huazhong University of science and technology. He obtained his Ph.D. in Ocean Engineering. His research interests are nonlinear dynamical fluid structure interaction systems applications in ocean and ship system control.

Dakui Feng is a lecturer and research fellow in School of Ocean Engineering, Huazhong University of science and technology. He obtained his Ph.D. in Ocean Engineering. His area of interest is ship hydrodynamics, ocean wave-structure interaction and wind engineering.